

# Magnetic Anchored CoPt Bimetallic Nanoparticles as Selective Hydrogenation Catalyst for Cinnamaldehyde

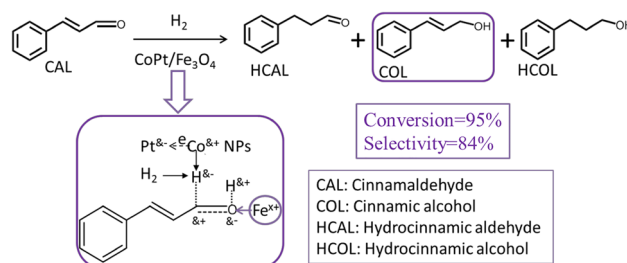
Tao Yuan<sup>1</sup> · Derong Liu<sup>1</sup> · Yue Pan<sup>1</sup> · Xiaoqin Pu<sup>1</sup> · Yongde Xia<sup>2</sup> · Jinbo Wang<sup>1</sup> · Wei Xiong<sup>1</sup>

Received: 9 August 2018 / Accepted: 18 November 2018  
© Springer Science+Business Media, LLC, part of Springer Nature 2018

## Abstract

Selective hydrogenation reaction of cinnamaldehyde is crucial for its application in fine chemical industries. The traditional noble metal catalyst for this reaction is expensive and often involving tedious steps. In this work, the magnetic anchored CoPt/Fe<sub>3</sub>O<sub>4</sub> catalyst is prepared by a simple wet-impregnation method and evaluated as catalyst for selective hydrogenation of cinnamaldehyde. Electrons transfer directly from Co to Pt NPs can enhance H<sub>2</sub> dissociation capability in the Co NPs interface, thereby strengthen the overall catalytic performance. Under optimum conditions, the conversion of cinnamaldehyde is 95% with 84% selectivity of cinnamyl alcohol. Furthermore, the magnetic interaction between the outer Co NPs and the Fe<sub>3</sub>O<sub>4</sub> support maintains the stability of cinnamyl alcohol selectivity after repeated tests.

## Graphical Abstract



**Keywords** CoPt/Fe<sub>3</sub>O<sub>4</sub> NPs · Electron transfer · Selective hydrogenation · Magnetic separation

## 1 Introduction

The limited availability of natural sources could not meet the widespread demand of fine chemicals especially for allyl alcohol in food, perfume and pharmaceutical industries during the past 20 years. Moreover, it is challenging for the traditional transformation of  $\alpha$ ,  $\beta$ -unsaturated aldehydes to obtain the allyl alcohols, because selective hydrogenation of the C=C bond is thermodynamically favoured. Noyori and co-workers invented the highly effective and homogeneous Ruthenium(II)-Phosphine-diamine catalytic system that could acquire high selectivity of C=O bond hydrogenation under mild conditions. However, the separation and recovery of the catalyst are still the key issues for industrialization. Based on previous works, researchers have investigated new solutions to tackle these problems such as phosphine and

**Electronic supplementary material** The online version of this article (<https://doi.org/10.1007/s10562-018-2619-6>) contains supplementary material, which is available to authorized users.

✉ Wei Xiong  
18875024416@163.com

<sup>1</sup> Institute of Chemistry and Chemical Engineering,  
Chongqing University of Science and Technology,  
Chongqing 401331, China

<sup>2</sup> College of Engineering, Mathematics and Physical Sciences,  
University of Exeter, Exeter EX4 4QF, UK

amine modification [1–5]. Recently, owing to the easy separation and high catalytic properties of the supported catalysts, most researchers focus on how to improve the single noble metal catalytic performance by adding a second metal (Sn, Fe, Co) [6–8] or metal oxides (FeOx, MoOx, CeOx, NbOx) [9–12] and selecting some suitable 2D (RGO, CNTs, SiC, PP-3) [13–16] or 3D (MS, MOFs, COFs) [17–19] nanoporous materials. Metal nanoparticles (NPs) are generally dispersed on these porous supports to maximize their availability, as porous materials can make advantageous contributions in restricting metal NPs mobility and preventing their leakage and sintering on some unfriendly reaction conditions. Moreover “Shape Selective Effect” in porous carrier can sharply raise the selectivity to C=O bond hydrogenation, which can screen the smaller steric hindrance aspect of substrate to pass through the aperture and react with the active components. Due to the ordered and tunable pores and diversified structures, MOF materials have been served as the best candidates for selective hydrogenation [20, 21]. Up to now, researchers have developed series of novel MOF catalysts such as NPs@MOFs [22], MOFs@NPs@MOFs [23], and COFs@NPs@MOFs [24] to effectively boost the C=O bond hydrogenation.

According to literature reports [25–27] the noble metals (Ir, Pt, Au) have been popular catalysts that are capable of enhancing catalytic efficiency in selective hydrogenation of  $\alpha$ ,  $\beta$ -unsaturated aldehyde but the catalytic processes are tedious and the catalysts are costly. In this regard, the nonprecious metal Co is an alternative catalyst with great potential in catalytic hydrogenation. Zhang et al [28], have employed ZSM-5 as carrier to support Co NPs to catalyze the selective hydrogenation of cinnamaldehyde (CAL), and the optimum cinnamic alcohol (COL) selectivity reaches 61.9%. Joseph et al. [29] have demonstrated that Co NPs impregnation on the reducible metal oxides show superiority in COL selectivity compared with the  $\gamma$ -Al<sub>2</sub>O<sub>3</sub>, SiO<sub>2</sub> and TiO<sub>2</sub>. The presence of TiO<sub>x</sub> ( $x < 2$ ) species have favourable promotion to selective hydrogenation of C=O groups. Bi-functional catalyst Co@CN from N-containing [Co(TPA)(ted)<sub>0.5</sub>] has achieved 99% COL selectivity with full conversion after 35 h [30]. The nitrogen-doped porous carbon materials (CPNs) [31] are excellent support to impregnate Co NPs, which demonstrates high catalytic performance with 99% conversion and 80% COL selectivity. Apart from the single Co catalyst, the Co–M alloy is efficient catalyst for selective hydrogenation of cinnamaldehyde. Kalyon et al. [32] have fabricated Co–B catalyst that could achieve remarkable selectivity to C=O group hydrogenation because of the special spiral structure of noncrystalline CoB. Moreover, when the CoB catalyst is modified by doping the transition metals Mo and W, the reaction rate and selectivity to unsaturated alcohol could be significantly improved by strengthening its structural stability [33].

Given that the non-precious Co shows low conversion at low temperature and low selectivity at high temperature [31], bimetallic CoPt NPs were synthesized to cope with the low catalytic efficiency by effectively modulating the electron state of the outer Co NPs (the electrons shift from Co to Pt NPs). In the meantime, the magnetic Fe<sub>3</sub>O<sub>4</sub> is employed as excellent carrier that is not only conducive to rapid magnetic separation after reaction, but also the Fe cations originating from the Fe<sub>3</sub>O<sub>4</sub> surface can act as the Lewis acid sites to interact with the C=O bond and lower the reaction-energy barrier [34, 35], which can contribute to the selective hydrogenation of C=O group, as shown in Graphical Abstract.

Meanwhile, to our knowledge, there have been no studies to explore the effect of magnetic interaction between Co NPs and Fe<sub>3</sub>O<sub>4</sub> on the product distribution for the hydrogenation of cinnamaldehyde transformation. In this work, we have fabricated magnetic anchored bimetallic CoPt/Fe<sub>3</sub>O<sub>4</sub> catalyst. The bimetallic CoPt NPs are chosen as the main catalytic active phase to convert cinnamaldehyde into unsaturated alcohol. The efficient electron transfer between Co and Pt NPs enhances Co NPs catalytic activity. The magnetic interactions between the outer Co NPs and Fe<sub>3</sub>O<sub>4</sub> support maintain the selectivity of unsaturated alcohol. Consequently, we have successfully achieved high catalytic performances of Co NPs at both low and high temperatures.

## 2 Experimental Section

### 2.1 Catalyst Preparation

The CoPt NPs were prepared following the literature [36] with minor modifications. Briefly, 2.6 mL HPtCl<sub>6</sub> aqueous solution (10 mM, Macklin), 300 mg PVP (K30, Macklin) and 20 mL H<sub>2</sub>O were continuously added to a 50 mL beaker. After the mixture was stirred at 800 rpm for 10 min until complete dissolving of the ingredients, 20 mL freshly prepared NaBH<sub>4</sub> aqueous solution (0.5 mg/mL, Kelong) was slowly dropwise added, and left for 20 min to form Pt nanoparticles. Then 2.6 mL Co(NO<sub>3</sub>)<sub>2</sub> aqueous solution (10 mM, Kelong) was introduced into the above solution and reacted for another 20 min to obtain CoPt bimetallic nanoparticles under stirring at 1500 rpm. All the synthesis steps were protected by N<sub>2</sub> atmosphere. Finally, 0.5 g PVP modified Fe<sub>3</sub>O<sub>4</sub> was added into the above solution and kept standing for 12 h. The resulting mixture was centrifuged and washed with distilled water several times, and then dried under vacuum at 80 °C for 24 h.

### 2.2 Catalyst Characterization

The Powder X-Ray diffraction (PXRD) scans of the synthesized CoPt/Fe<sub>3</sub>O<sub>4</sub> catalysts were carried out from 0° to 80°,

using an XRD-7000 X-ray diffractometer (CuK $\alpha$  radiation at 40 kV and 30 mA, Japan). The morphology and microstructure of the sample, the HAADF-STEM imaging and EDX mapping of CoPt/Fe<sub>3</sub>O<sub>4</sub> catalysts were recorded by a high resolution electron microscopy (200 KV, FEI Talos F200x, American) and the samples were supported by carbon coated copper grids. The elemental valence state and content of Fe, Co and Pt nanoparticles at the surface of Fe<sub>3</sub>O<sub>4</sub> were measured by X-ray photoelectron spectroscopy (XSAM800, UK), using a double anode Mg K $\alpha$  X-ray source (45 W) and an analyzer pass energy of 20 eV. The information of configuration of CoPt/Fe<sub>3</sub>O<sub>4</sub> was characterized using Temperature-programmed desorption and Temperature-programmed reduction (H<sub>2</sub>-TPD, H<sub>2</sub>-TPR, AutochemII 2920 (10 deg/min, 10% H<sub>2</sub>-Ar, 50 mL/min), American). The magnetic properties of sample were characterized using a vibrating sample magnetometer (VSM, lakeshore735, Germany).

### 2.3 Selective Hydrogenation Reaction

The hydrogenation reaction was performed in a 0.1 L stainless steel autoclave equipped with a magnetic stirrer. The detailed procedures are as follows: 0.8 mmol substrate, 5 mg catalyst doze and 5 mL i-PrOH were added into the stainless autoclave in turn. The autoclave was kept sealed under charging certain hydrogen after purging with nitrogen several times. Then the autoclave was heated to the pre-set temperature (100–180 °C) and the reaction started. After a period of reaction time, the autoclave was cooled down to room temperature and decompressed. The product of the final liquid was analyzed by an Agilent GC-6890N gas chromatography equipped with a FID detector and a Rtx-1 capillary column (30 m  $\times$  0.25 mm  $\times$  0.25  $\mu$ m) with N<sub>2</sub> as the carrier gas. The CAL conversion and product selectivity were calculated according to the following equations:

$$\text{Conversion} = \frac{\text{CAL before reaction} - \text{CAL after reaction}}{\text{CAL before reaction}} \times 100\%$$

$$\text{Selectivity} = \frac{\text{Desired product}}{\text{CAL consumed}} \times 100\% \quad (\text{all unit : mole})$$

## 3 Results and Discussion

### 3.1 Catalyst Characterization

To better understand the catalysts, they are fully characterized by XRD, TEM, XPS, H<sub>2</sub>-TP and VSM. The PXRD patterns of 1%CoPt/Fe<sub>3</sub>O<sub>4</sub> (1% define as the whole Co and Pt loading, Table S1) catalysts (n (Co/Pt) = 1/2, 1/1 and 2/1) are shown in Fig. 1. The main peaks at 2 $\theta$  around 18.3°, 30.1°, 35.5°, 37.1°, 43.1°, 53.4°, 57.0°, 62.6° and 75.1°,

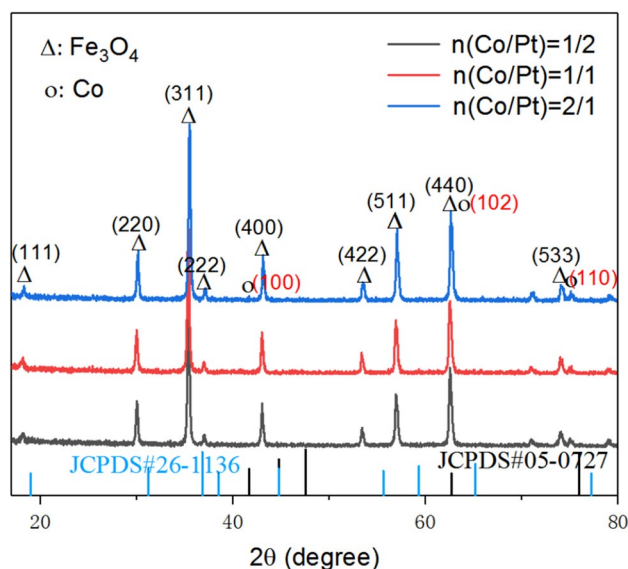


**Fig. 1** PXRD patterns of the CoPt/Fe<sub>3</sub>O<sub>4</sub> (1%) with different molar ratio of Co to Pt

correspond to the (111), (220), (311), (222), (400), (422), (511), (440) and (533) diffractions of iron oxide, respectively. Compared to the standard Iron oxide (JCPDS No.26-1136), the PXRD peaks of the catalyst are left shifted, which could be caused by the influence of the outer magnetic Co NPs on the iron oxide crystal phase [37]. Meanwhile, the weak characteristic Co peaks in accord with lower Co content occurring at 2 $\theta$  of 62.6° and 75.9° are assigned to (102) and (110) of Co respectively, which initially infers the presence of Co NPs. However, no characteristic diffraction peaks of Pt are observable from the single XRD analysis, which may be because the Pt clusters are fully covered by the outer Co NPs. Therefore, the high resolution transmission electron microscopy (HRTEM) was conducted to further validate the composition, morphology and microstructure of the CoPt/Fe<sub>3</sub>O<sub>4</sub> catalyst (as shown in Fig. 2). The mean particle size of the CoPt/Fe<sub>3</sub>O<sub>4</sub> is 173.7  $\pm$  35.4 nm. Its morphology shows cubic or spherical polyhedron, and the active ingredients (CoPt NPs) locate on the margin of Fe<sub>3</sub>O<sub>4</sub> polyhedron as shown in the red cycles in Fig. 2b. In addition, Fig. 2c shows that the formation CoPt morphology is similar to core-shell structure which is developed from a Pt cluster core. The thickness of outer Co NPs is estimated as 5.0–12.6 nm. In Fig. 2d, two different lattice spacing of approximately 0.148 and 0.286 nm are observed, which are originated from the Co (102) and Fe<sub>3</sub>O<sub>4</sub> (220) respectively. Finally, from the EDS elemental mapping in Fig. 2f–h, the presence of Fe, Co element are clearly observed and the blurring Pt mapping image in Fig. 2h further confirms the XRD results that the majority of Pt clusters is covered by the outer Co NPs.

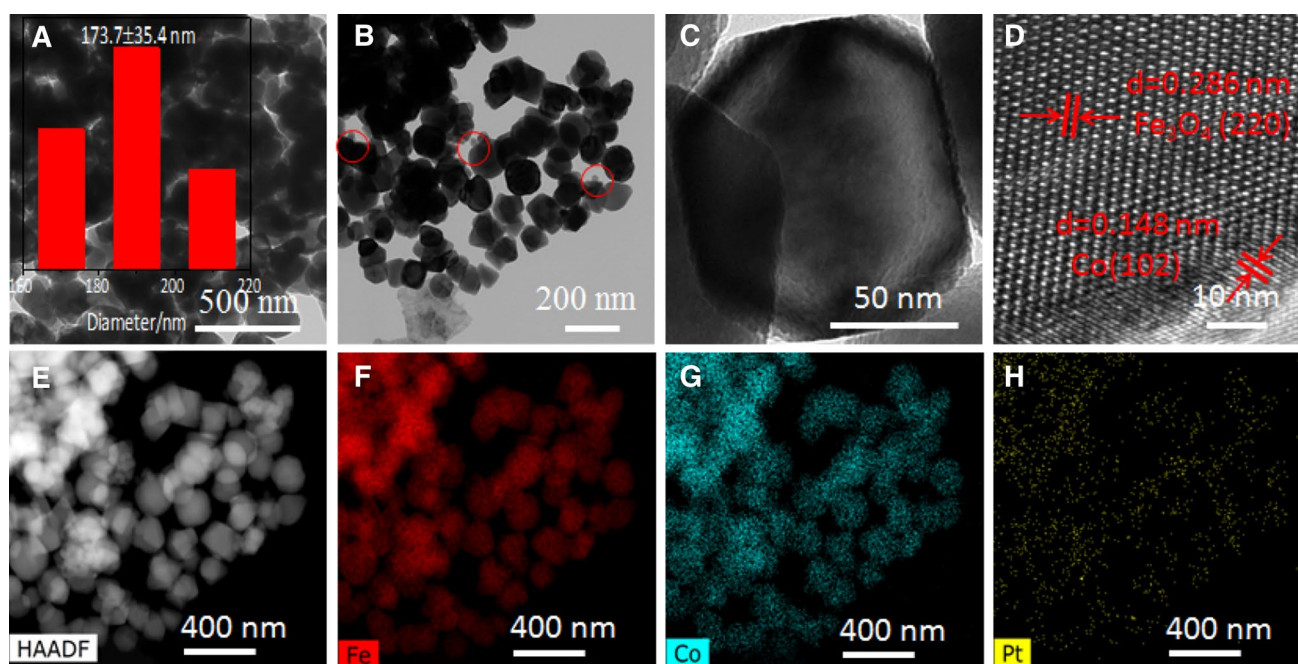
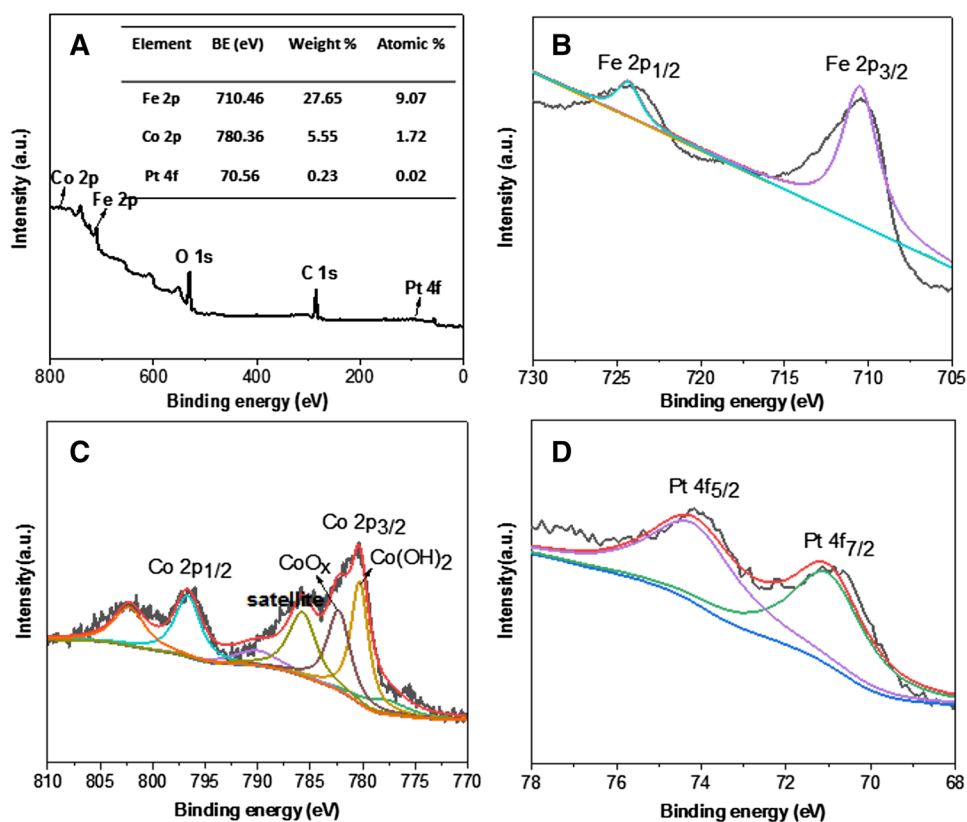


**Fig. 2** HRTEM images of CoPt/Fe<sub>3</sub>O<sub>4</sub> (1%) catalyst (**a, b, c, d**), **e** HAADF-STEM image, and elemental mapping for **f** Fe, **g** Co and **h** Pt

In an effort to understanding the content and valence of Co and Pt at the surface of Fe<sub>3</sub>O<sub>4</sub>, X-ray photoelectron spectrum of the CoPt/Fe<sub>3</sub>O<sub>4</sub> (1%) catalyst was employed.

From Fig. 3a (the elemental analysis result based on the XPS spectrum), due to the outer Co NPs, the XPS can't accurately detect the real core Pt content, which gives the

**Fig. 3** **a** XPS spectra of Pt@Co/Fe<sub>3</sub>O<sub>4</sub> (1%), **b** Fe 2p spectrum, **c** Co 2p spectrum, **d** Pt 4f spectrum



atomic ratio of Co/Pt = 1.72/0.02, far exceeding the original Co/Pt = 2/1. However, the elemental contents of Co and Pt from XPS analysis result are similar to their content derived from elemental mapping in EDS. In addition, the peak positions of Fe 2p<sub>3/2</sub> and Fe 2p<sub>1/2</sub> are, at 710.6 eV and 724.1 eV respectively, in agreement with the binding energy of standard of Fe<sub>3</sub>O<sub>4</sub> [38]. For Co species, the doubling peaks at binding energy of 802.5 and 782.2 eV are attributed to the chemical environment of Co 2p<sub>1/2</sub> and Co 2p<sub>3/2</sub> from CoO<sub>x</sub>, due to the oxidation of the Co shell after exposure to air atmosphere. The other pair of doubling peaks for Co 2p<sub>1/2</sub> and Co 2p<sub>3/2</sub> from Co(OH)<sub>2</sub> appeared at binding energy of 796.2 and 780.4 eV, which are validated by published reports [33, 36]. In addition, a satellite peak can be found at around 785.5 eV. Considering the typical peak position of Co 2p<sub>3/2</sub> for Co(OH)<sub>2</sub> is at 780.9 eV, it is clearly that this peak in the catalyst is left shifted, which implies the Co layer is losing electron. In addition, the Pt 4f<sub>7/2</sub> binding energy for Pt<sup>0</sup> is at 70.6 eV that is evidently reduced by 0.4 eV compared with the typical Pt<sup>0</sup> peak position at 71.0 eV, indicating the electrons shift from the Co to Pt NPs [39]. The Co NPs with electron deficiency could be benefit the high catalytic activity in the reaction of cinnamaldehyde transformation.

To investigate the configuration of CoPt/Fe<sub>3</sub>O<sub>4</sub> catalyst, the H<sub>2</sub>-TPD and H<sub>2</sub>-TPR characterization were conducted. The analysis result displays that there exist two peaks of H<sub>2</sub> desorption in the H<sub>2</sub>-TPD profile (Fig. 4a). The first peak of obvious H<sub>2</sub> desorption centre appears at 440 °C, which is consistent with the CoO<sub>x</sub> [40]. Another broad and weak peak locates between 600 and 800 °C which indicates that Fe<sub>3</sub>O<sub>4</sub> support was reduced [41]. From the H<sub>2</sub>-TPR profile (Fig. 4b), the first-stage reduction temperature locates at 388 °C which is lower than Co<sub>2</sub>O<sub>3</sub> or Co<sub>3</sub>O<sub>4</sub> reduction temperature [42]. It demonstrates that there exists interaction between Pt and CoO<sub>x</sub> causing by the hydrogen spillover, which results in the

reduction of CoO<sub>x</sub> shifting to lower temperature since the metallic Pt atoms are able to dissolve hydrogen molecules into hydrogen atom [40, 42].

### 3.2 Optimization of Reaction Conditions

Various reaction conditions including temperature, H<sub>2</sub> pressure, duration and solvent types were investigated for optimization. The influence of temperature on the selective hydrogenation of cinnamaldehyde is presented in Fig. 5a. The conversion of cinnamaldehyde has sharply increased from 14 to 95% with increasing temperature until 160 °C. Afterwards, the conversion starts to decrease. Surprisingly, the COL selectivity does not change significantly and largely holds at 81–88%. The selectivity of HCAL and HCOL shows in an opposite way, the selectivity of HCAL declines from 8 to 2% while that for HCOL increases from 5 to 17%. Moreover, the effect of hydrogen pressure on the catalytic activity is depicted in Fig. 5b. The conversion goes up from 68 to 95% with the hydrogen pressure changing from 2 to 3 MPa, which reveals that the hydrogen pressure increase is beneficial to the conversion. Unfortunately, the COL selectivity reduces from 87 to 81% slightly. The HCAL and HCOL selectivity is in line with the trend of the temperature influence. As shown in Fig. 5c, the reaction duration mainly influences the CAL conversion. With duration extending to 180 min, the conversion increases from 65 to 95%. However, the COL selectivity slightly changes (only 4% fluctuation). In addition, Fig. 5d implies that the polar solvents such as alcohols are beneficial to the C=O group selective hydrogenation, as the carbonyl group tends to form hydrogen bonds in alcohols, thus enhancing the polarization of the carbonyl group and in favor of the carbonyl group selective hydrogenation. Among those alcohols, i-PrOH has the highest conversion up to 95% with 84% COL selectivity

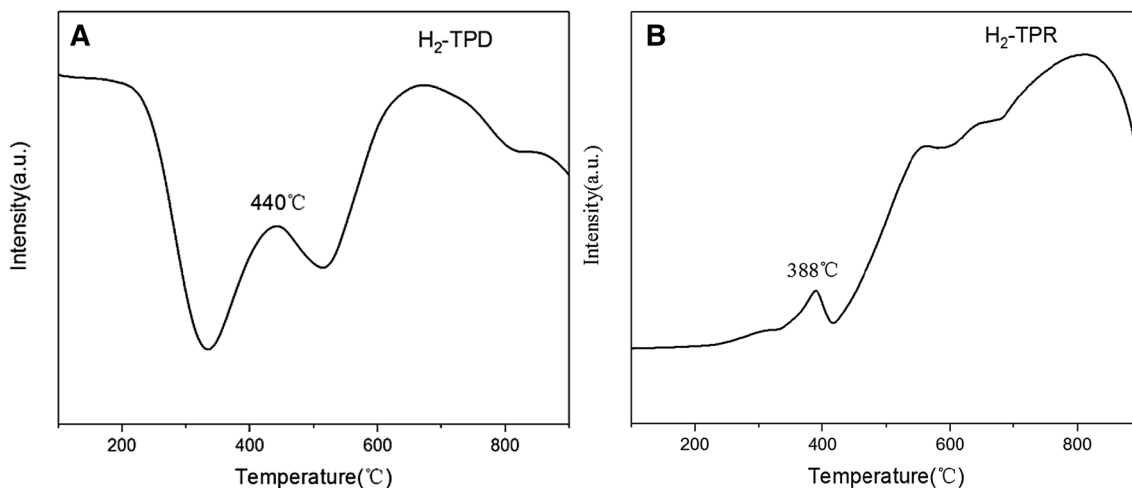


**Fig. 4** The H<sub>2</sub>-TP profiles of CoPt/Fe<sub>3</sub>O<sub>4</sub> catalyst, **a** H<sub>2</sub>-TPD and **b** H<sub>2</sub>-TPR

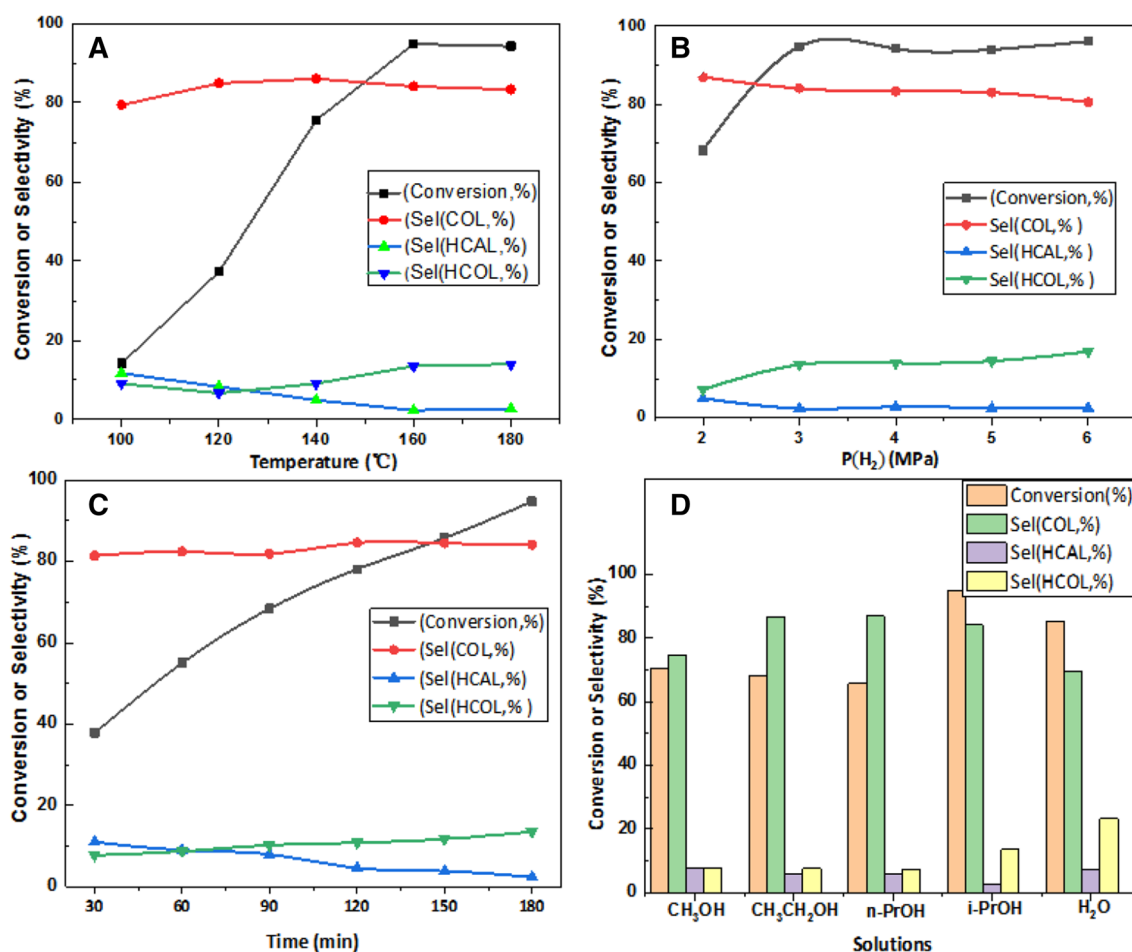


**Fig. 5** The optimization of reaction conditions of CoPt/Fe<sub>3</sub>O<sub>4</sub> (1% (n (Co/Pt)=2/1)) catalyst including temperature (**a**), H<sub>2</sub> pressure (**b**), duration (**c**) and solution type (**d**). **a** Reaction condition: 5 mg catalyst dose, 5 mL i-PrOH, 0.8 mmol substrate, 180 min, P(H<sub>2</sub>)=3 MPa, **b** reaction condition: 5 mg catalyst dose, 5 mL i-PrOH, 0.8 mmol

substrate, 160 °C, 180 min, **c** reaction condition: 5 mg catalyst dose, 5 mL i-PrOH, 0.8 mmol substrate, 160 °C, P(H<sub>2</sub>)=3 MPa, **d** reaction condition: 5 mg catalyst dose, 0.8 mmol substrate, 160 °C, 180 min, P(H<sub>2</sub>)=3 MPa

than other alcohols, which indicates that the alcohol's spatial structure could influence the yield including both conversion and selectivity. Apart from the optimization of reaction conditions, the stability and recycling possibility of the prepared catalysts in selective hydrogenation of cinnamaldehyde are investigated in detail (ESI, Fig. S1). There is no observable change of COL selectivity and it maintains unchanged at around 84%, even after five successive tests.

### 3.3 Activities of Various Catalysts

Based on the above results, the optimized reaction conditions (temperature, pressure, etc.) were adopted for further study. Different catalysts in the reaction of selective hydrogenation of cinnamaldehyde have been systematically studied and the catalytic performances are listed in Table 1 (Entry 1–6). The conversion of the single magnetic anchored Co/Fe<sub>3</sub>O<sub>4</sub> catalyst only reaches 7% with 13% of COL selectivity. After

adding the Pt atom, significant increase in the conversion of cinnamaldehyde is observed for the PtCo/Fe<sub>3</sub>O<sub>4</sub> catalyst (8%) and the CoPt/Fe<sub>3</sub>O<sub>4</sub> catalyst (27%).

Obviously, the CoPt/Fe<sub>3</sub>O<sub>4</sub> catalyst exhibited much higher catalytic performances and its conversion achieves 3.8 times and the COL selectivity 6.6 times of those of the single Co/Fe<sub>3</sub>O<sub>4</sub> catalyst, respectively. This indicates that the presence of Pt acting as the core is capable of enhancing the catalytic activity. Furthermore, the CoPt/Fe<sub>3</sub>O<sub>4</sub> catalytic conversion is slightly superior to the Pt/Fe<sub>3</sub>O<sub>4</sub> catalyst. Among the studied different catalyst supports, the magnetic Fe<sub>3</sub>O<sub>4</sub> support exhibits the highest selectivity of 84% with respect to the  $\gamma$ -Al<sub>2</sub>O<sub>3</sub> (68%) and TiO<sub>2</sub> (71%) supports. The main reason lies in that the Fe cation efficiently interacts with the C=O group and activates it at the surface of Fe<sub>3</sub>O<sub>4</sub>. Meanwhile, the catalytic performance of the diverse magnetic catalysts M-Pt/Fe<sub>3</sub>O<sub>4</sub> (M is Fe, Co, Ni, and n(M/Pt)=1/1) is further investigated and the results are also listed in Table 1 (Entry

**Table 1** Comparison of different catalysts in selective hydrogenation of cinnamaldehyde under various conditions

Entry	Catalysts	Conv. (%)	S <sub>COL</sub> (%)	S <sub>H<sub>2</sub>COL</sub> (%)	S <sub>H<sub>2</sub>COL</sub> (%)
1	1% Co/Fe <sub>3</sub> O <sub>4</sub> <sup>A</sup>	7	13	15	0
2	1% Pt/Fe <sub>3</sub> O <sub>4</sub> <sup>A</sup>	24	88	7	4
3	1% PtCo/ Fe <sub>3</sub> O <sub>4</sub> <sup>A</sup>	8	75	25	0
4	1% CoPt/ Fe <sub>3</sub> O <sub>4</sub> <sup>A</sup>	27	84	10	7
5	1% CoPt/ $\gamma$ - Al <sub>2</sub> O <sub>3</sub> <sup>A</sup>	41	68	23	10
6	1% CoPt/ TiO <sub>2</sub> <sup>A</sup>	18	71	20	10
7	1% FePt/ Fe <sub>3</sub> O <sub>4</sub> <sup>B</sup>	16	89	11	0
8	1% NiPt/ Fe <sub>3</sub> O <sub>4</sub> <sup>B</sup>	90	39	26	36
9	1% CoPt/ Fe <sub>3</sub> O <sub>4</sub> <sup>B</sup>	51	84	9	7
10	1% CoPt/ Fe <sub>3</sub> O <sub>4</sub> <sup>C</sup> n(Co/Pt)=1/2)	29	84	12	3
11	1% CoPt/ Fe <sub>3</sub> O <sub>4</sub> <sup>C</sup> n(Co/Pt)=1/1)	51	84	9	7
12	1% CoPt/ Fe <sub>3</sub> O <sub>4</sub> <sup>C</sup> n(Co/Pt)=2/1)	95	84	2	14

<sup>A</sup>Reaction conditions: 5 mg catalyst dose, 5 mL i-PrOH, 0.8 mmol substrate, 120 °C, 120 min, A<sup>3,4,5,6</sup>(n(Co/Pt)=1/1)

<sup>B</sup>Reaction condition: 5 mg catalyst dose, 5 mL i-PrOH, 0.8 mmol substrate, 160 °C, 180 min, (n(M/Pt)=1/1)

<sup>C</sup>Reaction condition: 5 mg catalyst dose, 5 mL i-PrOH, 0.8 mmol substrate, 160 °C, 180 min

7–9). The CoPt/Fe<sub>3</sub>O<sub>4</sub> catalyst shows excellent catalytic activity and the conversion is up to 95% with 84% COL selectivity. However, it is noticeable that totally different catalytic results are observed for FePt/Fe<sub>3</sub>O<sub>4</sub> catalyst and NiPt/Fe<sub>3</sub>O<sub>4</sub> catalyst. The FePt/Fe<sub>3</sub>O<sub>4</sub> catalyst has high COL selectivity of 89% with low conversion of 16%. Conversely, the conversion of NiPt/Fe<sub>3</sub>O<sub>4</sub> reaches 97% with COL selectivity of only 39%. These catalytic results are closely link with the electron arrangement in d orbits of the M metals. The Fe NPs has the higher holes in 3d energy bands which can be acted as electron acceptor, it can therefore efficiently interact with C=O groups in CAL to boost its hydrogenation.

However, the Fe NPs is against H<sub>2</sub> dissociation and results in low conversion. Rather, the Ni NPs is in favour of H<sub>2</sub> dissociation but lacks of the capability of activating C=O groups, thereby leading to the hydrogenation of C=C groups. Additionally, different molar ratio of Co/Pt greatly influences the catalytic efficiency of the CoPt/Fe<sub>3</sub>O<sub>4</sub> catalysts as shown in Table 1 (Entry 10–12). With increasing

Co content, the reaction conversion has sharply ascended from 29 to 95%, but the selectivity of COL keeps almost constant. Further study is required to deep insight into the relevant phenomenon occurring in the selectivity which is not yet fully understood. Other Co based catalysts in recent published references is displayed in ESI Table S2. As non-precious Co metal is chosen as the active ingredients, the Co loading and catalyst dosage is far higher than noble metal catalysts. Moreover, the Co based catalysts have low catalytic activity at low temperature and needs long reaction time. Meanwhile, it is hard to achieve high selectivity of unsaturated alcohol at high temperatures. However, adding trace amount of Pt to form CoPt NPs is capable of enhancing the catalytic activity. Even if the reaction is carried out at 160 °C, the CoPt/Fe<sub>3</sub>O<sub>4</sub> catalyst still shows excellent selectivity of COL (84%).

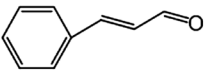
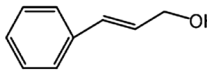
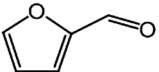
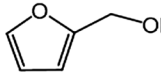
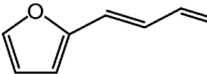
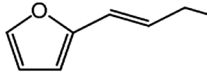
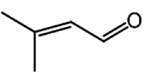
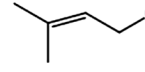
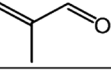
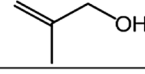
Table 2 presents the selective hydrogenation of various  $\alpha$ ,  $\beta$ -unsaturated aldehydes with CoPt/Fe<sub>3</sub>O<sub>4</sub> (1%) catalyst. From Table 2, it is clear that  $\alpha$ ,  $\beta$ -unsaturated aldehydes with different substituents greatly affect the conversion and selectivity of the reaction turning them into unsaturated alcohol. The cinnamaldehyde conversion is up to 95% with 84% COL selectivity. But for furfural, the conversion is only 24%, which may be closely related to the strength of conjugated aromaticity. Furfural is more stable than cinnamaldehyde in the conjugated aromatic structure, so reaction of the conjugated C=O bond is more challenging for selective hydrogenation. Besides, the types of branched chain and the position of branched chain of  $\alpha$ ,  $\beta$ -unsaturated aldehyde are other important factors which influence the final products of the selective hydrogenation.

Finally, the vibrating sample magnetometer (VSM) of CoPt/Fe<sub>3</sub>O<sub>4</sub> (1%) before and after reaction was measured. For clarity, the magnetization hysteresis loop of CoPt/Fe<sub>3</sub>O<sub>4</sub> (1%) is presented in Fig. 6. The saturation magnetization of the CoPt/Fe<sub>3</sub>O<sub>4</sub> catalyst is 93.6 emu/g. After five successive tests, its saturation magnetization slightly declines but still shows 79.7 emu/g. This suggests that the catalyst remains favourable magnetic separation performance when it is dispersed into the ethanol solution again.

## 4 Conclusions

The magnetic Fe<sub>3</sub>O<sub>4</sub> is employed as support for effective anchoring bimetallic CoPt NPs by a simple wet-impregnation method. The prepared CoPt/Fe<sub>3</sub>O<sub>4</sub> (1%) catalyst exhibits excellent catalytic performance in hydrogenation of CAL with conversion up to 95% and COL selectivity of 84%. Moreover, the prepared CoPt/Fe<sub>3</sub>O<sub>4</sub> catalyst remains excellent magnetic separation performance even after five successive tests. Under optimized experimental conditions, the conversion is greatly affected by the different

**Table 2** Selective hydrogenation of different  $\alpha$ ,  $\beta$ -unsaturated aldehydes with CoPt/Fe<sub>3</sub>O<sub>4</sub> (1%) catalyst

Entry	Substrate	Product	Conv.(%)	S <sub>COL</sub> (%)
1			95	84
2			95	24
3			96	76
4			86	40
5			29	96

Reaction conditions: 5 mg catalyst dose, 5 mL i-PrOH, 0.8 mmol substrate, 160 °C, 180 min, P(H<sub>2</sub>) = 3 MPa

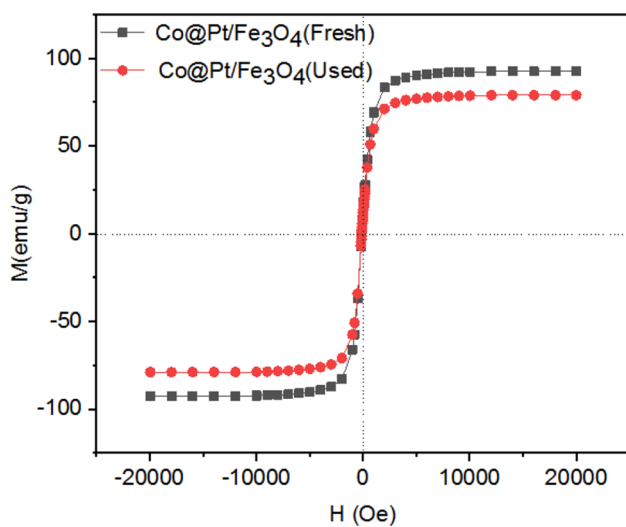


**Fig. 6** The magnetization hysteresis loop of the CoPt/Fe<sub>3</sub>O<sub>4</sub> (1%) catalyst before and after reaction

variables, but COL selectivity largely keeps unchanged, due to the strong magnetic interactions between the outer Co nanoparticles and Fe<sub>3</sub>O<sub>4</sub> support.

**Acknowledgements** The authors are grateful for the financial support from the Basic and Frontier Research Project of Chongqing in China (No. cstc2016jcyjA0139). Moreover, I very much appreciate my tutors for giving many precious suggestions about how to conduct experiments and write article.

## Compliance with Ethical Standards

**Conflict of interest** The authors declare that they have no conflict of interest.

## References

- Chen X, Zhu H, Song X, Du H, Wang T et al (2017) Ru-PPh<sub>3</sub>@porous organic polymer: efficient and stable catalyst for the trickle bed regioselective hydrogenation of cinnamaldehyde. *React Kinet Mech Catal* 120:637–649
- Gombos R, Joó F (2014) Selective hydrogenation of cinnamaldehyde and phospholipids in aqueous-organic biphasic systems with ruthenium(II) complex catalysts. *Green Process Synth* 3:127–132
- Ali HA, Al-Noaimi MZ, Mahmoud SS (2015) Selective hydrogenation of cinnamaldehyde catalyzed by ruthenium(II) complexes based on azoimine ligands. *Jordan J Chem* 10:58–68
- Prokopchuk DE, Morris RH (2012) Inner-sphere activation, outer-sphere catalysis: theoretical study on the mechanism of transfer hydrogenation of ketones using iron(II) PNNP enamide complexes. *Organometallics* 31:7375–7385
- Mager N, Libioulle P, Carlier S, Hermans S (2017) Water-soluble single source precursors for homo- and hetero-metallic nanoparticle catalysts supported on nanocarbons. *Catal Today* 301:153–163
- Dietrich C, Schild D, Wang W, Kübel C, Behrens S (2017) Bimetallic Pt/Sn-based nanoparticles in ionic liquids as nanocatalysts for the selective hydrogenation of cinnamaldehyde. *Z Anorg Allg Chem* 643:120–129
- Liu Z, Tan X, Li J, Lv C (2013) Easy synthesis of bimetal PtFe-containing ordered mesoporous carbons and their use as catalysts for selective cinnamaldehyde hydrogenation. *New J Chem* 37:1350–1357
- Zheng Q, Wang D, Yuan F, Han Q, Dong Y et al (2016) An effective co-promoted platinum of Co-Pt/SBA-15 catalyst for selective hydrogenation of cinnamaldehyde to cinnamyl alcohol. *Catal Lett* 146:1535–1543

9. Hu Q, Wang S, Gao Z, Li Y, Zhang Q et al (2017) The precise decoration of Pt nanoparticles with Fe oxide by atomic layer deposition for the selective hydrogenation of cinnamaldehyde. *Appl Catal B* 218:591–599
10. He S, Xie L, Che M, Chan HC, Yang L et al (2016) Chemoselective hydrogenation of  $\alpha,\beta$ -unsaturated aldehydes on hydrogenated MoOx nanorods supported iridium nanoparticles. *J Mol Catal A* 425:248–254
11. Bhogeswararao S, Srinivas D (2012) Intramolecular selective hydrogenation of cinnamaldehyde over CeO<sub>2</sub>-ZrO<sub>2</sub>-supported Pt catalysts. *J Catal* 285:31–40
12. Tamura M, Tokonami K, Nakagawa Y, Tomishige K (2017) Effective NbOx-modified Ir/SiO<sub>2</sub> catalyst for selective gas-phase hydrogenation of crotonaldehyde to crotyl alcohol. *ACS Catal* 5:3685–3697
13. Ji XW, Niu XY, Li B, Han Q, Yuan FL et al (2014) Selective hydrogenation of cinnamaldehyde to cinnamal alcohol over platinum/graphene catalysts. *ChemCatChem* 6:3246–3253
14. Ni X, Zhang B, Li C, Pang M, Su D et al (2012) Microwave-assisted green synthesis of uniform Ru nanoparticles supported on non-functional carbon nanotubes for cinnamaldehyde hydrogenation. *Catal Commun* 24:65–69
15. Yao R, Li J, Wu P, Li X (2016) The superior performance of a Pt catalyst supported on nanoporous SiC-C composites for liquid-phase selective hydrogenation of cinnamaldehyde. *RSC Adv* 6:81211–81218
16. Bhanja P, Liu X, Modak A (2017) Pt and Pd nanoparticles immobilized on amine-functionalized hypercrosslinked porous polymer nanotubes as selective hydrogenation catalyst for  $\alpha,\beta$ -unsaturated aldehydes. *ChemistrySelect* 2:7535–7543
17. Wang D, Zhu Y, Tian C, Wang L, Zhou W et al (2016) Synergistic effect of Mo<sub>2</sub>N and Pt for promoted selective hydrogenation of cinnamaldehyde over Pt-Mo<sub>2</sub>N/SBA-15. *Catal Sci Technol* 6:2403–2412
18. Chen L, Zhan W, Fang H, Cao Z, Yuan C et al (2017) Selective catalytic performances of noble metal nanoparticle@MOF composites: the concomitant effect of aperture size and structural flexibility of MOF matrices. *Chem Eur J* 23:11397–11403
19. Li H, Pan Q, Ma Y, Guan X, Xue M et al (2016) Three-dimensional covalent organic frameworks with dual linkages for bifunctional cascade catalysis. *J Am Chem Soc* 138:14783–14788
20. Luz I, Rösler C, Epp K, Llabrés i Xamena FX (2015) Pd@UiO-66-type MOFs prepared by chemical vapor infiltration as shape-selective hydrogenation catalysts. *Eur Inorg Chem* 2015:3904–3912
21. Zhang N, Shao Q, Wang P, Zhu X, Huang X (2018) Porous Pt-Ni nanowires within in situ generated metal-organic frameworks for highly chemoselective cinnamaldehyde hydrogenation. *Small* 14:1704318
22. Guo Z, Xiao C, Maligalanes RV, Zhou L, Tian WG et al (2014) Pt nanoclusters confined within metal-organic framework cavities for chemoselective cinnamaldehyde hydrogenation. *ACS Catal* 4:1340–1348
23. Zhao M, Yuan K, Wang Y, Li G, Guo J et al (2016) Metal-organic frameworks as selectivity regulators for hydrogenation reactions. *Nature* 539:76–80
24. Yuan K, Song T, Wang D, Zhang X, Gao X et al (2018) Effective and selective catalysts for cinnamaldehyde hydrogenation: hydrophobic hybrids of metal-organic frameworks, metal nanoparticles, and micro- and mesoporous polymers. *Angew Chem Int Ed* 57:5708–5713
25. Masazumi T, Dai Y, Teruhisa O, Yoshinao N, Keiichi T (2017) In-situ formed Fe cation-modified Ir/MgO catalyst for selective hydrogenation of unsaturated carbonyl compounds. *ACS Catal* 7:5103–5111
26. Song S, Liu X, Li J, Pan J, Wang F et al (2017) Confining the nucleation of Pt to in situ form (Pt-enriched cage)@CeO<sub>2</sub> core@shell nanostructure as excellent catalysts for hydrogenation reactions. *Adv Mater* 29:1700495
27. Chen H, Cullen DA, Lares JZ (2015) Highly efficient selective hydrogenation of cinnamaldehyde to cinnamyl alcohol over gold supported on zinc oxide materials. *J Phys Chem C* 119:28885–28894
28. Zhang B, Zhang XB, Xu LY, Zhang YJ, Qin YH et al (2013) Selective hydrogenation of cinnamaldehyde over ZSM-5 supported Co catalysts. *React Kinet Mech Catal* 110:207–214
29. Joseph Antony Raj K, Prakash MG, Elangovan T, Viswanathan B (2011) Selective hydrogenation of cinnamaldehyde over cobalt supported on alumina, silica and titania. *Catal Lett* 142:87–94
30. Liu X, Cheng S, Long J, Zhang W, Liu X et al (2017) MOFs-derived Co@CN bi-functional catalysts for selective transfer hydrogenation of  $\alpha,\beta$ -unsaturated aldehydes without use of base additives. *Mater Chem Front* 1:2005–2012
31. Jiang P, Gao W, Wang X, Tang Y, Lan K, Wang B et al (2017) Highly selective hydrogenation of  $\alpha,\beta$ -unsaturated carbonyl compounds over supported Co nanoparticles. *Catal Commun* 111:6–9
32. Kalyon N, Hofmann K, Malter J, Lucas M, Claus P et al (2017) Catalytic activity of nanoscale borides: Co<sub>2</sub>B and Ni<sub>2</sub>B<sub>3</sub> in the liquid-phase hydrogenation of citral. *J Catal* 352:436–441
33. Mo M, Zheng M, Tang J, Lu Q, Xun Y (2013) Highly active Co-B, Co-Mo(W)-B amorphous nanotube catalysts for the selective hydrogenation of cinnamaldehyde. *J Mater Sci* 49:877–885
34. Pan H, Li J, Lu J, Wang G, Xie W et al (2017) Selective hydrogenation of cinnamaldehyde with PtFe<sub>x</sub>/Al<sub>2</sub>O<sub>3</sub>@SBA-15 catalyst: enhancement in activity and selectivity to unsaturated alcohol by Pt-FeOx and Pt-Al<sub>2</sub>O<sub>3</sub>@SBA-15 interaction. *J Catal* 354:24–36
35. Zhang Y, Chen C, Gong W, Song J (2017) Chemoselective transfer hydrogenation of cinnamaldehyde over activated charcoal supported Pt/Fe<sub>3</sub>O<sub>4</sub> catalyst. *Chin J Chem Phys* 30:467–473
36. Liu Y, Fang Z, Kuai L, Geng B (2014) One-pot facile synthesis of reusable tremella-like M1@M2@M1(OH)<sub>2</sub> (M1 = Co, Ni, M2 = Pt/Pd, Pt, Pd and Au) three layers core-shell nanostructures as highly efficient catalysts. *Nanoscale* 6:9791–9797
37. Guo M, Balamurugan J, Li X, Kim NH, Lee JH (2017) Hierarchical 3D cobalt-doped Fe<sub>3</sub>O<sub>4</sub> nanospheres@NG hybrid as an advanced anode material for high-performance asymmetric supercapacitors. *Small* 13:1701275
38. Yamashita T, Hayes P (2008) Analysis of XPS spectra of Fe<sup>2+</sup> and Fe<sup>3+</sup> ions in oxide materials. *Appl Surf Sci* 254:2441–2449
39. Gu Y, Zhao Y, Wu P, Yang B, Yang N, Zhu Y (2016) Bimetallic Pt<sub>x</sub>Co<sub>y</sub> nanoparticles with curved faces for highly efficient hydrogenation of cinnamaldehyde. *Nanoscale* 8:10896–10901
40. Wang X, He Y, Liu Y, Park J, Liang X. Atomic layer deposited Pt-Co bimetallic catalysts for selective hydrogenation of  $\alpha,\beta$ -unsaturated aldehydes to unsaturated alcohols. *J Catal* 366:61–69
41. Tu J, Ding M, Wang T, Ma L, Xu Y, Kang S, Zhang G (2017) Direct conversion of bio-syngas to gasoline fuels over a Fe<sub>3</sub>O<sub>4</sub>@C Fischer-tropsch synthesis catalyst. *Energy Procedia* 105:82–87
42. Silva D, Luza L, Gual A, Baptista D et al (2014) Straightforward synthesis of bimetallic Co/Pt nanoparticles in ionic liquid: atomic rearrangement driven by reduction-sulfidation processes and Fischer-Tropsch catalysis. *Nanoscale* 6:9085–9092